

# A Unified Deep Semantic Expansion Framework for Domain-Generalized Person Re-identification

Eugene P.W. Ang, Shan Lin\* and Alex C. Kot

Rapid-Rich Object Search (ROSE) Lab, Nanyang Technological University, School of EEE, 50 Nanyang Ave S2-B4b-13, 639798, Singapore

## ARTICLE INFO

### Keywords:

Person Re-Identification  
Image Retrieval  
Domain Generalization  
Deep Feature Semantic Expansion

## ABSTRACT

Supervised Person Re-identification (Person ReID) methods have achieved excellent performance when training and testing within one camera network. However, they usually suffer from considerable performance degradation when applied to different camera systems. In recent years, many Domain Adaptation Person ReID methods have been proposed, achieving impressive performance without requiring labeled data from the target domain. However, these approaches still need the unlabeled data of the target domain during the training process, making them impractical in many real-world scenarios. Our work focuses on the more practical Domain Generalized Person Re-identification (DG-ReID) problem. Given one or more source domains, it aims to learn a generalized model that can be applied to unseen target domains. One promising research direction in DG-ReID is the use of implicit deep semantic feature expansion, and our previous method, Domain Embedding Expansion (DEX), is one such example that achieves powerful results in DG-ReID. However, in this work we show that DEX and other similar implicit deep semantic feature expansion methods, due to limitations in their proposed loss function, fail to reach their full potential on large evaluation benchmarks as they have a tendency to saturate too early. Leveraging on this analysis, we propose Unified Deep Semantic Expansion, our novel framework that unifies implicit and explicit semantic feature expansion techniques in a single framework to mitigate this early over-fitting and achieve a new state-of-the-art (SOTA) in all DG-ReID benchmarks. Further, we apply our method on more general image retrieval tasks, also surpassing the current SOTA in all of these benchmarks by wide margins.

## 1. Introduction

Person re-identification, also known as Person ReID, is the task of matching images or videos of the same person over a multi-camera surveillance system. Many fully supervised models already demonstrate impressive performance when trained and tested on the same dataset. However, most of these models often over-fit the training dataset (the source surveillance system) and usually suffer from considerable performance degradation when tested on unseen datasets (the target surveillance system). To address the large domain gap between source and target domains, many recent works utilize domain adaptation (DA) techniques to enhance the model's cross-domain capability. However, DA methods require target domain images/videos to adapt to the target system, which, in many real-world scenarios, is difficult to get. As a result, DA-ReID methods constrain the applicability of Person ReID and may delay system deployment.

Our work in this paper follows the more practical Domain Generalization (DG) approach. Domain Generalized Person Re-identification, also known as DG-ReID, focuses on training a generalized model from multiple existing datasets without any prior knowledge of or access to the target domain. This is a more practical scenario for several reasons. Firstly, supervised or domain-adaptation methods require an extra round of retraining or adaptation when presented with a new domain. However, not all stakeholders are able to provide the resources for such retraining or adaptation as these methods take significant time and

hardware to train [1, 2]. Furthermore, it may not be feasible to access data from the new domain because of privacy issues, necessitating that the method be unaware of the target domain [1]. Finally, for large scale commercialization it is ideal to offer solutions that can work out-of-the-box without extra fine-tuning or retraining, as not all stakeholders have the resources to do so [3].

Various techniques of DG-ReID such as meta-learning [1], hyper-networks [3] and memory banks [2] have greatly advanced the state-of-the-art. Furthermore, a recent class of implicit semantic feature expansion methods has emerged [4, 5] that have shown promise in DG-ReID. Implicit semantic expansion methods emerge naturally as a resource-light alternative to explicit semantic expansion. Performing explicit semantic expansion on raw images and deep features [6, 7, 8] injects more semantic variety to a fixed dataset of images and can be viewed as a form of data augmentation. However, instead of explicitly manipulating the raw image or feature, implicit semantic methods encode this explicit semantic expansion into differentiable loss functions. As these loss functions are theoretical constructs, they are intractable to compute. Thus, current works on implicit semantic expansion derive surrogate upper bounds of these ideal losses and optimize those instead. Implicit semantic expansion methods yield strong results in DG-ReID and are simple to implement, usually consisting of a loss function that plugs naturally into a standard deep neural network architecture such as a ResNet-50 [9].

Our previous method, Domain Embedding EXpansion (DEX) [10], is one such application of implicit semantic expansion specialized toward DG-ReID, and this work aims

\*Corresponding author

Email addresses: phuaywee001@e.ntu.edu.sg (E.P.W. Ang); shan.lin@ntu.edu.sg (S. Lin); eackot@ntu.edu.sg (A.C. Kot)

to improve on our previously published method by addressing its limitations and increasing its capability. Performing a detailed analysis of DEX, we discover an interesting phenomenon: the DEX loss function causes inter-class distances in the final classifier layer to shrink. Combined with the dynamics of the DEX loss, this shrinkage reduces constraints on the parameters to be learnt, resulting in a complex model with a higher tendency to over-fit. Thus, the theoretical benefits of implicit semantic expansion are offset by this tendency to over-fit and prevent DEX from reaching its full potential. Experiments on inter-class weight distances are presented in Figure 2, while details of our analysis of the issue are discussed in subsection 3.2.

To overcome this limitation, we propose a crucial enhancement: by performing explicit semantic expansion along with the implicit, we can mitigate the shrinkage of inter-class distances during training and extend the runway of improvement during training.

Our method, **Unified Deep Semantic EXpansion (UDSX)**, accommodates both implicit and explicit semantic expansion by proposing three major framework innovations.

Firstly, **Data Semantic Decoupling (DSD)** streams the data into two independent pathways during training, allowing each stream to specialize in implicit or explicit semantic expansion without cross-interference from the other stream. The additional independent explicit semantic expansion stream creates an extra loss function component to mitigate the shrinkage of inter-class distances.

Secondly, a progressive expansion schedule, **Progressive Spatio-Temporal Expansion (PSTE)**, moderates the explicit semantic expansion process, allowing expansion to take place progressively and in targeted feature channels. This stabilizes training during the application of explicit semantic expansion, which if not carefully controlled could degrade performance.

Finally, a reunification component, **Contrastive-Stream Reunification (CSR)**, recombines the two independent semantic expansion streams. CSR consists of a trio of loss functions, **Contrastive-Stream Pairwise Loss (CSP)**, **Contrastive-Stream Center Loss (CSC)**, and **Contrastive-Stream Triplet Loss (CST)**, which enforce stream-invariance of features while maintaining class consistency. Instances from both streams, having gone through different semantic expansion processes, are trained to retain pertinent features that remain invariant to their particular streams. At the same time, these stream-invariant features are encouraged to maintain inter-class alignment so that features within the same class remain aligned with one another.

With this proposed design, UDSX achieves significantly higher test performance in all major DG-ReID benchmarks. Further, we demonstrate that UDSX performs well in more general image retrieval benchmarks, significantly surpassing the SOTA in benchmarks such as CUB-200-2011 (CUB) [11], Stanford-Cars (Cars196) [12], VehicleID [13] and Stanford Online Products (SOP) [14].

To summarize, our contributions are as follows:

1. We uncover a limitation of DEX, our current state-of-the-art (SOTA) implicit semantic expansion method in DG-ReID. We analyze this limitation, which also applies to other implicit expansion methods, and use our analysis to propose a resolution;
2. We design a dual-stream framework for decoupling and reunifying explicit and implicit semantic expansions. It is simple to implement, addresses the limitations of previous methods and further boosts DG-ReID performance to the next level. To the best of our knowledge, UDSX is the first method to unify implicit and explicit semantic expansion in training;
3. Our new method, UDSX, outperforms existing SOTA methods in various DG-ReID benchmarks by large margins;
4. UDSX also outperforms the SOTA on more general image retrieval tasks such as CUB-200-2011, Stanford Cars, VehicleID and Stanford Online Products for methods with a ResNet-50 backbone architecture;

## 2. Related Work

### 2.1. Domain Adaptation Person ReID

Supervised Person ReID methods [15, 16, 17, 18] have shown impressive accuracy in same-domain benchmarks, but these methods overfit to the training domain (dataset) and generalize poorly on different domains. Domain Adaptation Person ReID (DA-ReID) addresses this issue by training models to *adapt* to differences between source and target domains. DA-ReID models are trained on the labeled source domain data and utilize the attributes or styles of the unlabeled target domain data to perform adaptation. Recent DA-ReID methods exploit GAN-based image-synthesis [19], domain alignments [20, 21], pseudo labels [22] and memory banks [23, 24, 25] to close the gap between source and target domains. Although DA-ReID approaches have yielded good performance in recent years, these methods still require a large amount of data from the target domain. It severely affects the model's applicability in the real-world, where access to target domain data is not always possible.

### 2.2. Domain Generalization Person ReID

Domain Generalization Person ReID (DG-ReID) aims to learn a model that can perform well in unseen target domains without involving any target domain data for adaptation. DualNorm [26] first introduced the instance normalization (IN) layer to automatically normalize the style and content variations within the image batch during the training. MMFA-AAE [21] used a domain adversarial learning approach to remove domain-specific features. Later DG methods such as DIMN [3], QAConv [2] and M<sup>3</sup>L [1] used hyper-networks or meta-learning frameworks coupled with memory bank strategies. ACL [27] proposed a module to separately process domain invariant and domain specific features, plugging the module to replace selected convolutional blocks. RaMoE [28] and META [29] deploy a mixture of experts to specialize to each domain. Style

Interleaved Learning (SIL) [30] is a framework with a regular forward/backward pass, with one additional forward pass that employs style interleaving on features to update class centroids. Part-Aware Transformer [31] learns locally similar features shared across different IDs, further using the part-guided information for self-distillation. Different from the above approaches, which require substantial architectural or framework modifications, applying implicit semantic expansion only requires replacing the cross-entropy loss with a modified loss that encodes the implicit semantic expansion process, without requiring network manipulation or complex training frameworks. Thus, implicit semantic expansion losses can be easily applied to any deep neural network architecture and yield strong results in DG-ReID benchmarks.

### 2.3. Implicit Deep Feature Semantic Expansion

Recent works [32, 4, 5] discovered that it was possible to alter the semantics (e.g., color, shape, orientation) of images by shifting their encoded deep features in specific directions. DeepAugment [32] designed an image-to-image model to create novel and semantically meaningful image samples to boost the training set. Implicit semantic data augmentation methods [4, 5] go a step further by cutting away the extraneous image-to-image generation and instead generate new and semantically meaningful samples *in feature space*. They rely on class-level deep feature statistics to direct the perturbations in feature space while preserving class label information. DEX [10] tailored this approach for the DG-ReID problem by semantically expanding the deep features along *domain-wise* directions instead of class-wise directions. We performed a detailed analysis of the implicit semantic expansion loss of the DEX method and discovered a limitation of this technique for the DG-ReID problem. Based on our discovery, we proposed UDSX: a dual-stream framework that accommodates both explicit and implicit semantic expansion techniques to boost the model’s generalization ability. We present our analysis in the following section.

## 3. Background

### 3.1. Domain Embedding Expansion

Our previous method, Domain Embedding Expansion (DEX), is an implicit deep feature expansion technique that improves cross-domain feature representation learning. It is specially adapted to close domain gaps in multi-domain generalization problems. Like other such methods [33, 32, 5], the DEX loss function implicitly perturbs features in semantically meaningful directions sampled from per-domain feature statistics. DEX is a perfect drop-in replacement for the identity classification loss of standard Person ReID baselines and is an efficient way to perform semantic expansion without having to explicitly manipulate feature semantics. Figure 1 presents a high level overview of DEX.

The DEX loss presented in our previous paper is derived as such. Given a feature extractor  $f$  with classifier layer

weights  $\mathbf{w}$ , consider the cross-entropy loss of a single sample  $\mathbf{x}$  with label  $y$ :

$$\mathcal{L}_{CE} = -\log \left( \frac{e^{\mathbf{w}_y \cdot f(\mathbf{x})}}{\sum_{j=1}^C e^{\mathbf{w}_j \cdot f(\mathbf{x})}} \right), \quad (1)$$

where  $C$  is the number of unique person identities indexed by  $j$ . Biases are omitted in our classifier layer. The design rationale behind DEX is derived from [5]. Given that  $\mathbf{x}$  comes from domain  $d$ , we consider the *expected* softmax loss if the deep features were projected along domain-level covariance directions  $\Sigma_d$ :

$$\begin{aligned} \mathcal{L}_\infty &= \mathbb{E}_{\widetilde{f(\mathbf{x})}} \left[ -\log \left( \frac{e^{\mathbf{w}_y \cdot \widetilde{f(\mathbf{x})}}}{\sum_{j=1}^C e^{\mathbf{w}_j \cdot \widetilde{f(\mathbf{x})}}} \right) \right] \\ &= \mathbb{E}_{\widetilde{f(\mathbf{x})}} \left[ \log \left( \sum_{j=1}^C e^{(\mathbf{w}_j - \mathbf{w}_y) \cdot \widetilde{f(\mathbf{x})}} \right) \right], \end{aligned} \quad (2)$$

where  $\widetilde{f(\mathbf{x})} \sim \mathcal{N}(f(\mathbf{x}), \lambda \Sigma_d)$  are the projected features assumed to be normally distributed around  $f(\mathbf{x})$  with domain-conditional covariance  $\Sigma_d$ , and  $\lambda \geq 0$  controls the magnitude of the projection. Applying Jensen’s Inequality,  $\mathbb{E}[\log(X)] \leq \log(\mathbb{E}[X])$ , we can move the logarithm out of the expectation to get:

$$\mathcal{L}_\infty \leq \log \left( \sum_{j=1}^C \mathbb{E}_{\widetilde{f(\mathbf{x})}} e^{(\mathbf{w}_j - \mathbf{w}_y) \cdot \widetilde{f(\mathbf{x})}} \right) \quad (3)$$

We apply the moment generating function  $\mathbb{E}[\exp(tX)] = \exp(t\mu + \frac{1}{2}\sigma^2 t^2)$ ,  $X \sim \mathcal{N}(\mu, \sigma^2)$ , substituting  $t$  with  $(\mathbf{w}_j - \mathbf{w}_y)$  and  $X \sim \mathcal{N}(\mu, \sigma^2)$  with  $\widetilde{f(\mathbf{x})} \sim \mathcal{N}(f(\mathbf{x}), \lambda \Sigma_d)$ , to derive our loss:

$$\mathcal{L}_{DEX} = -\log \left( \frac{e^{\mathbf{w}_y \cdot f(\mathbf{x})}}{\sum_{j=1}^C e^{\mathbf{w}_j \cdot f(\mathbf{x}) + \frac{\lambda}{2} (\mathbf{w}_j^T - \mathbf{w}_y^T) \Sigma_d (\mathbf{w}_j - \mathbf{w}_y)}} \right) \quad (4)$$

$\mathcal{L}_{DEX}$  is an upper bound to the *expectation* of cross-entropy loss over infinitely perturbing  $f(\mathbf{x})$  in directions determined by per-domain covariance matrix  $\Sigma_d$ . In theory, optimizing  $\mathcal{L}_{DEX}$  reaps the benefits of semantic data expansion while avoiding the overheads of having to perform the computation explicitly.

### 3.2. DEX Loss Function Limitations

We observed a unique behavior of models trained with the DEX loss. While achieving strong generalization performance, the best validation performance of these models is achieved very quickly at lower epochs (Table 1), showing

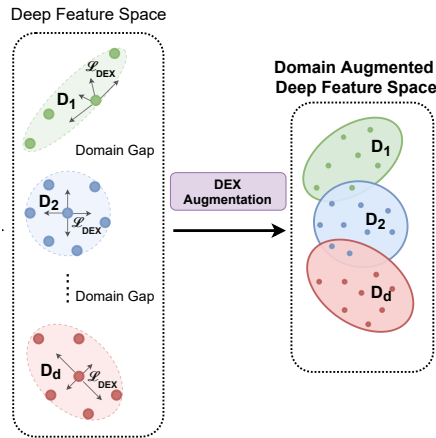


**Figure 1:** DEX, our adaptation of implicit semantic expansion to DG-ReID. DEX improves exploration of the domain space by implicitly projecting training points in the directions of the domain distribution.

that it over-fits to the source datasets at an early stage. This phenomenon occurs consistently in all benchmarks we tested. In contrast, if we replace the DEX loss with a baseline person identity cross-entropy loss, the performance improves for much longer before over-fitting, even though it ultimately reaches a lower performance. A question naturally arises from this observation: is it possible to circumvent this limitation of the DEX loss and allow it to continue improving beyond this limit? In this follow-up study, we analyze the DEX loss and formulate a hypothesis about the cause behind this behavior. To rectify this, we design a method that unifies both implicit and explicit semantic expansion processes and allows the model to further improve in generalization.

For the purposes of this analysis, we can simplify the DEX loss from Equation 4 as such:

$$\mathcal{L}_{DEX} = -\log\left(\frac{e^{\mathbf{w}_y \cdot f(\mathbf{x})}}{\sum_{j=1}^C e^{\mathbf{w}_j \cdot f(\mathbf{x}) + \Gamma}}\right) \quad (5)$$

Where  $\Gamma = \frac{\lambda}{2}(\mathbf{w}_j^T - \mathbf{w}_y^T)\Sigma_d(\mathbf{w}_j - \mathbf{w}_y)$ . Recast in this form, we can see that the DEX loss is simply the original cross-entropy (CE) loss for identity classification with an extra term added for each value in the denominator sum. The first crucial thing to observe is that the covariance matrix  $\Sigma_d$  is positive semi-definite, which implies that  $\Gamma \geq 0$ , since  $\lambda$  is non-negative. Similar to CE loss, the DEX loss maximizes the similarity between feature and true-class weights in the numerator and minimizes the denominator. But in order to minimize the denominator, Equation 5 has to minimize  $\Gamma$ . To do this, it has to minimize the difference between  $w_y$  and  $w_j$ , which encourages class weights to be close to each other. Consider the scenario where all class weight vectors  $w_j$  have converged very closely to one another. Given an input  $\mathbf{x}$  of label  $y$ , the backbone extractor  $f$  would have to exaggerate the magnitude of  $f(\mathbf{x})$  in order for  $\mathbf{w}_y \cdot f(\mathbf{x})$  in the numerator to be greater than  $\mathbf{w}_{j \neq y} \cdot f(\mathbf{x})$  in the denominator.  $f$  is

**Table 1**

Best epochs and scores on C+D+MS  $\rightarrow$  M over values of  $\lambda$  (see Sec 7.1 for benchmark details)

$\lambda$	Best Epoch	mAP	Rank-1
No DEX ( $\lambda = 0$ )	57	54.0	79.8
<b>5</b>	<b>39</b>	<b>54.8</b>	<b>81.1</b>
15	39	54.2	80.2
25	35	54.1	79.7
50	34	52.7	78.1

encouraged to learn weights of larger magnitude, undoing the weight-decay regularization that tries to constrain model parameters, and we are left with a complex backbone model that over-fits early as an unintended side effect of optimizing the DEX loss. Table 1 shows that applying DEX is effective, but too much of it rapidly degrades performance, and that the scores saturate faster as the DEX loss strength increases. Figure 2 plots and compares the maximum inter-class weight distances over time for DEX as we vary its strength. As we increase the strength of DEX through the hyperparameter  $\lambda$ , we observe the inter-class weight distances shrinking.

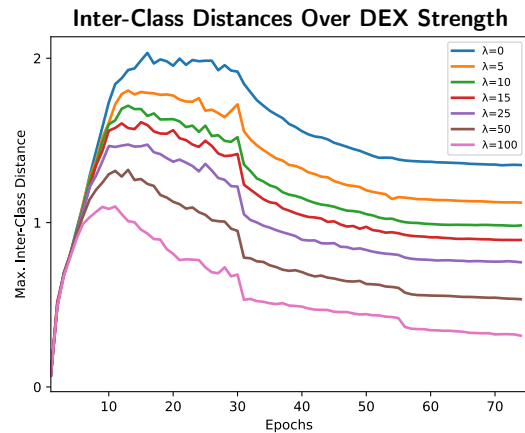


**Figure 2:** Increasing DEX strength decreases the distance between class weights. Best viewed in color.

#### 4. Integrating Explicit Semantic Expansion

A way to alleviate the issue described in the previous section would be to reduce the hyperparameter  $\lambda$ . However, Table 1 shows that setting  $\lambda$  too low also hurts performance; the extra  $\Gamma$  term improves results albeit with the cost of early over-fitting. Implicit semantic expansion methods were formulated as upper bounds of an idealized loss, and the deviation between the upper bound and the true loss ( $L_\infty$ ) is one of the main contributors of this limitation. We propose to add explicit semantic feature expansion to restore freedom to the inter-class weights and reach a closer approximation to the idealized loss. From the robustness literature, it is well known that injecting features with noise during training can improve model generalization [7, 34]. Building on this, we design an explicit semantic expansion method that computes

feature statistics at the domain level and uses these statistics to apply the explicit semantic expansion on features in a targeted way.

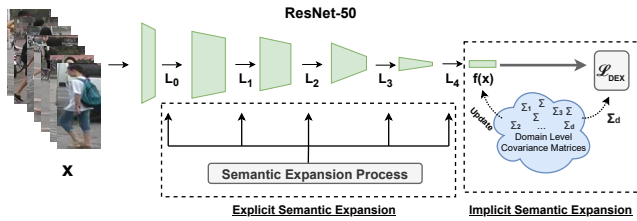


**Figure 3:** Naively combining explicit and implicit semantic expansion yields poor results as they disrupt each other.

A naive way to combine both implicit and explicit semantic expansion would be to perform both in conjunction as the model trains, as shown in Figure 3. However, we found that this did not improve performance and was detrimental in some cases, as Table 8 shows. By prematurely expanding the semantics of the intermediate features, we alter the distribution of the resultant feature embeddings that are fed to the DEX loss, thereby disrupting the learning of the implicit semantic loss. This over-coupling of implicit and explicit expansion processes constrains the model and renders it incapable of fully benefiting from both types of expansion. Instead, our proposed Unified Deep Semantic Expansion (UDSX) synergizes the strengths of both types of semantic expansion and enables the model to train for extended periods and improve past previous limits. UDSX comprises three framework innovations:

- Data Semantic Decoupling (DSD)
- Progressive Spatio-Temporal Expansion (PSTE)
- Contrastive-Stream Reunification (CSR)

### 4.1. Data Semantic Decoupling

Observing that explicit semantic expansion interferes with DEX, we designed a framework to better accommodate both types of expansion so that they can work together. Given a batch of data, we duplicate its contents into two streams and process them separately such that each stream receives the same content while having the flexibility to apply independent training conditions. Our twin data stream framework, Data Semantic Decoupling (DSD), is shown in Figure 4. With this modification, the DEX stream trains with DEX loss without interference from the explicit stream, and vice versa. The backbone model’s weights are shared between both data streams during training; during inference, DSD is disabled as only one stream is required to produce the output features.

### 4.2. Progressive Spatio-Temporal Expansion

We denote our proposed explicit semantic expansion process by the symbol  $P$ : given a feature  $\mathbf{x}$ ,  $P(\mathbf{x})$  represents the output of applying our explicit semantic expansion on  $\mathbf{x}$ . More details are provided in the following subsections. In subsection 4.2.1, we describe the process

of generating perturbations conditioned on the domain of the input and adding them to intermediate features. Next, in subsection 4.2.2, we describe the progression of semantic expansion across intermediate model layers over the course of training using our Progressive Temporal Expansion (PTE). Finally, we describe our Activation-Based Stratification (ABS) in subsection 4.2.3, which applies explicit semantic expansion on intermediate tensors in a controlled and localized manner that harmonizes with the backbone network’s learning dynamics.

#### 4.2.1. Domain Conditional Explicit Semantic Expansion Process

The intermediate features of the backbone are the targets of the explicit semantic expansion. We dynamically compute feature statistics of intermediate layers of the model by tracking and updating on-the-fly the per-element variances of each intermediate feature:  $V_{k \in \{0,1,2,3,4\}}^d$ , with  $k$  indexing the intermediate layers of the backbone ResNet-50 and  $d$  indexing the domain of the sample. We sample a zero-mean Gaussian using these variances conditioned on domain  $d$ , obtaining semantically meaningful perturbations which are added in a controlled manner to the intermediate features at layer- $k$ .

#### 4.2.2. Progressive Temporal Expansion (PTE)

We target the semantic expansion to be applied progressively on lower to higher layers over time. This design is guided by the observation that models first learn to encode low-level concepts such as textures, edges, shapes and colors in early layers before combining them into higher-order semantic abstractions in later layers. We harmonize with this natural order of development, randomly selecting from lower layers to expand at the start of training and progressively including higher layers over time. To moderate the amount of semantic change at any time, our policy randomly selects only one layer to perform semantic expansion at each forward pass.

#### 4.2.3. Activation-Based Stratification (ABS)

In order to maintain a controlled level of semantic change, we perturb only selected channels, or strata, of the intermediate tensor based on their average activation values. The stratification is specified for each intermediate layer as they each have different numbers of channels. Early layers have fewer channels compared to later layers, so a narrower band of channels would be selected for semantic expansion. Channels are sorted and selected according to their average activation values and selected only if these values fall within a defined quantile. Our stratified design allows for flexibility, allowing us to apply semantic expansion in a targeted way. In our specific case we select the middle quantile of channels whose average activation values fall within the top  $[\frac{3}{8}C_k, \frac{5}{8}C_k]$ , where  $C_k$  is the number of channels in the  $k$ -th intermediate tensor. In other words, we skip the channels with average activation values in the top and bottom quartiles. The intuition behind this design is that

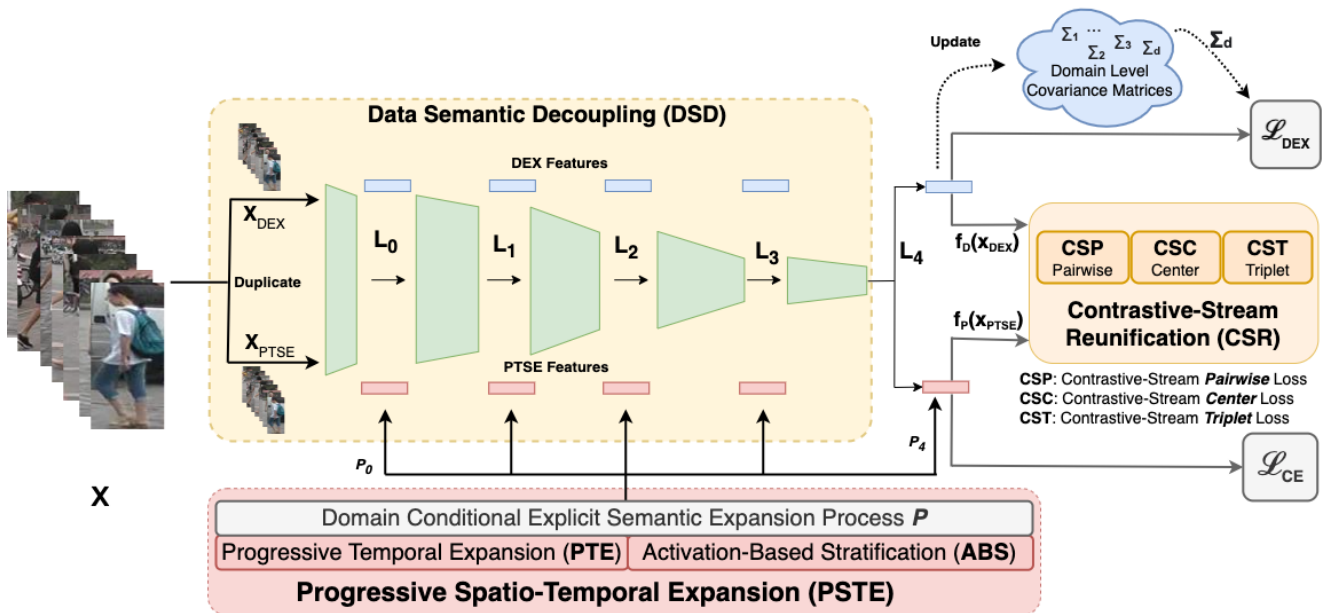


**Figure 4:** Our method UDSX unifies implicit and explicit semantic expansion in 3 parts: (1) Data Semantic Decoupling (DSD) isolates Domain Embedding Expansion (DEX) and Progressive Spatio-Temporal Expansion (PSTE) into dedicated streams, (2) PSTE is the engine behind the explicit semantic expansion, and (3) Contrastive-Stream Reunification (CSR) reunifies the streams at the end and more details on this component are illustrated in Figure 6. Best viewed in color.

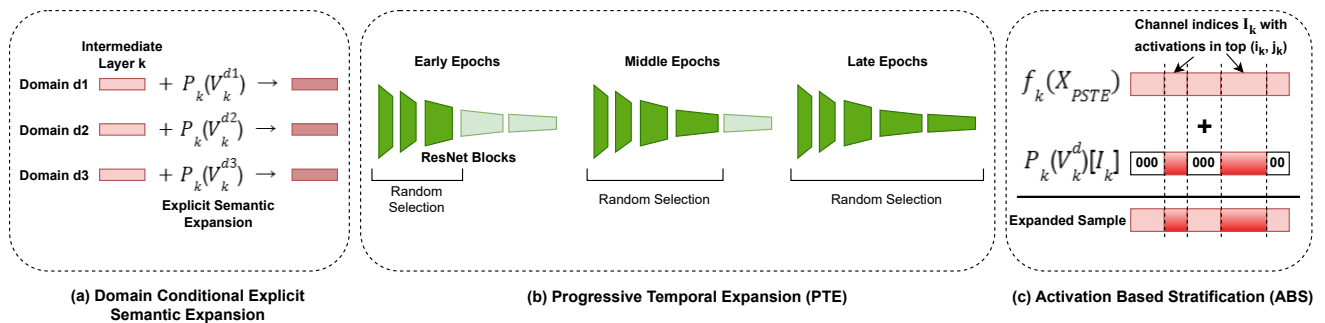


**Figure 5:** Components of PSTE illustrated. (a) Intermediate features are perturbed based on the domain that they come from, allowing the semantics of each domain to be better explored over time. (b) PTE: We start by randomly selecting among early intermediate features to perturb, and gradually over time expand the selection set to the later layers as the model begins to understand higher-level semantics. (c) ABS: Only selected channels are perturbed, based on their activation values falling within a pre-defined quantile: channels that are either very important or meaningless are left unperturbed. For more details, refer to Section 4.2 and Algorithm 1

the channels with the highest average activation values could contain important semantic information and should not be disrupted, while the lowest activated channels are unlikely to contain meaningful semantic information for expansion.

#### 4.2.4. Overview of Components

Figure 5 illustrates the core ideas behind PSTE. In (a), we convey the idea that each intermediate feature is explicitly expanded using a domain-conditional perturbation as described in subsection 4.2.1. In (b), we illustrate the progressive and temporal nature of PTE, where the perturbations are only randomly applied in early layers at the start of training and expand to the later layers as the model learns to encode higher-order semantics. In (c), we illustrate

how ABS is used to select channels for semantic expansion based on their activation values.

In more detail, Algorithm 1 describes how PSTE is applied to a sample input during a forward pass. Having randomly selected an intermediate layer  $k$  to perform the expansion, given an input  $x$  from domain  $d$  we intercept the intermediate feature  $x_k$  at layer- $k$  and rank their channels according to their average activation values to get the top  $i_k$ -to- $j_k$  highest channel indices  $I_k = \Lambda(x_k, i_k, j_k)$ . Using the stored variances  $\Sigma_{d,k}$ , we sample an expansion direction and add it to  $x_k$  only at the desired channel indices, finally deriving the expanded sample  $P(x_k) = x_k + \mathcal{N}(0, \Sigma_{d,k})_{I_k}$ .

**Algorithm 1** Progressive Spatio-Temporal Expansion (PSTE). In all our experiments, we fix  $R$  to be a uniform random selector. The channel activation sorter  $\Lambda$  abstracts the process of ranking the channels of an intermediate tensor  $x_k$  by their average activation values and returning the indices to the  $i_k$ -th to  $j_k$ -th largest channels (for  $i_k < j_k$ ).

**Abbreviations:**

SE=Semantic Expansion (See 4.2.1)

PTE=Progressive Temporal Expansion (See 4.2.2)

ABS=Activation-Based Stratification (See 4.2.3)

**Definitions**

$\mathbf{x}$ : Input image,

$d$ : Domain of  $\mathbf{x}$ ,

$f$ : Backbone model,

$V$ : Per-element variances,

$\mathcal{N}$ : Gaussian model,

$L$ : Ordered list of layer indices,

$\mu$ : Minimum layer width,

$t$ : Current epoch,

$T$ : Num epochs for PSTE,

$R$ : Random selector

$S$ : Top-k strata for each intermediate layer

$\Lambda$ : Average channel activation sorter

```

1: // PTE: select one layer from candidate layers based on
   stage of training.
2:  $l \leftarrow (|L| - 1) \times \min(\lfloor \frac{l}{T} \rfloor, 1)$  // Get last index
3:  $l \leftarrow \max(l, \mu)$  // Ensure min selection width
4:  $k \leftarrow R(L[0, \dots, l])$  // Choose one layer only
5: // ABS: apply SE only on pre-defined target channels
   based on per-channel activation values.
6:  $(i_k, j_k) \leftarrow S(k)$  // Strata for layer-k,  $i_k \leq j_k$ 
7:  $\mathbf{x}_k \leftarrow f_{:k}(\mathbf{x})$  // Intermediate output at k
8:  $I_k \leftarrow \Lambda(\mathbf{x}_k, i_k, j_k)$  // Top- $i_k$ -to- $j_k$  channel indices
9:  $\mathbf{x}_k[I_k] \leftarrow \mathbf{x}_k[I_k] + \mathcal{N}(0, \sqrt{V_k^d})[I_k]$ 
10: return

```

## 5. Contrastive-Stream Reunification

After the passing through the backbone model, features are compared across DEX and PSTE streams using our Contrastive-Stream Reunification (CSR) module to teach the model to reconcile cross-stream differences and extract key relevant information. CSR is a combination of three losses: Contrastive-Stream Pairwise (CSP) Loss, Contrastive-Stream Center (CSC) Loss and Contrastive-Stream Triplet (CST) Loss, all of which operate across DEX and PSTE streams to achieve this goal. CSP encourages the learning of expansion-invariant features, while CSC and CST create a more challenging metric learning environment for the model to learn similarities between corresponding samples across streams. Figure 6 sketches an overview of the components of CSR Loss.

### 5.1. Contrastive-Stream Pairwise Loss

In order to encourage the model to resolve the differences between features derived from the DEX and PSTE streams, we apply a  $L_1$  distance loss between pairs of duplicated samples that have each passed through different streams. Given  $f_D(\mathbf{x})$  and  $f_P(\mathbf{x})$  are global features from the implicit and explicit streams of the base model  $f$  respectively, our **Contrastive-Stream Pairwise Loss (CSP)** is defined as:

$$L_{CSP}(f, \mathbf{x}) = \|f_D(\mathbf{x}) - f_P(\mathbf{x})\|_1 \quad (6)$$

### 5.2. Contrastive-Stream Center Loss

Next, we apply a modified center loss, our **Contrastive-Stream Center Loss (CSC)**, to encourage the model to learn expansion-invariant feature representations. Given a batch of  $m$  samples  $\mathbf{x}$  with labels  $\mathbf{y}$  and batch-wise class centroids  $\mathbf{c}^{\mathbf{y}_i} = \frac{1}{m} \sum_{i=1}^m f(\mathbf{x}_i)$ , the original center loss [35] has the following form:

$$L_{Cen}(f, \mathbf{x}, \mathbf{y}) = \sum_{i=1}^m \|f(\mathbf{x}_i) - \mathbf{c}^{\mathbf{y}_i}\|_2 \quad (7)$$

In CSC, our loss is the distance between each sample  $\mathbf{x}$  and the class centroid from its *opposing* stream:

$$L_{CSC}(f, \mathbf{x}, \mathbf{y}) = \sum_{i=1}^m \|f_D(\mathbf{x}_i) - \mathbf{c}_P^{\mathbf{y}_i}\|_2 + \quad (8)$$

$$\sum_{i=1}^m \|f_P(\mathbf{x}_i) - \mathbf{c}_D^{\mathbf{y}_i}\|_2 \quad (9)$$

where  $\mathbf{c}_D^{\mathbf{y}_i} = \frac{1}{m} \sum_{i=1}^m f_D(\mathbf{x}_i)$ ,  $\mathbf{c}_P^{\mathbf{y}_i} = \frac{1}{m} \sum_{i=1}^m f_P(\mathbf{x}_i)$  are the centroids from the DEX and PSTE streams respectively.

### 5.3. Contrastive-Stream Triplet Loss

Finally, we apply our own variant of the triplet loss [36]. Given a feature extractor  $f$ , a distance metric  $\delta$ , and a triplet  $\mathbf{t} = (a, p, n)$  where  $a$  and  $p$  are from the same class and  $n$  is from a different class,  $[\delta_{f(a), f(p)} - \delta_{f(a), f(n)}]_+$  computes the triplet loss. Our **Contrastive-Stream Triplet Loss (CST)** loss is designed to optimize similarity in corresponding features from opposing streams. Given two feature extractors  $f$  and  $g$ , we define the cross-extractor triplet loss  $L_{XT}$  as:

$$L_{XT}(f, g, d, \mathbf{t}) = [\delta_{f(a), g(p)} - \delta_{f(a), f(n)}]_+ \quad (10)$$

We then define the Contrastive-Stream Triplet Loss as follows:

$$L_{CST}(f, \mathbf{x}, \mathbf{y}, \delta, \mathbf{T}) = \frac{1}{2} \mathbb{E}_{\mathbf{t} \in \mathbf{T}(\mathbf{x}, \mathbf{y})} [L_{XT}(f_D, f_P, \delta, \mathbf{t}) + L_{XT}(f_P, f_D, \delta, \mathbf{t})] \quad (11)$$

where  $\mathbf{T}(\mathbf{x}, \mathbf{y})$  is a set of triplets we obtain by applying Batch-Hard example mining [36].

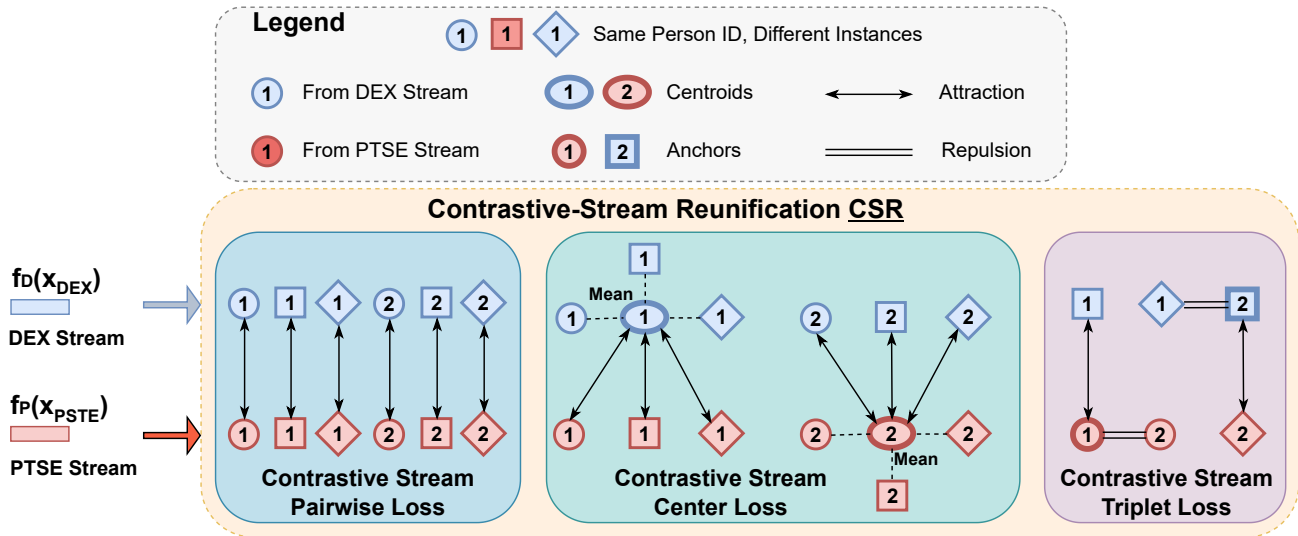


Figure 6: Overview of our Contrastive-Stream Reunification (CSR) Loss.

In forcing anchor and positive samples to be from opposite streams while anchor and negative are taken from the same stream, our Contrastive-Stream Triplet Loss increases the difficulty of the triplet optimization task and further encourages the features to be invariant to both explicit and implicit semantic expansions.

With non-negative weights  $\psi_1, \psi_2, \psi_3$  to control the strength of each loss component, the **Cross-Stream Reunification (CSR)** loss is:

$$L_{CSR} = \psi_1 L_{CSP} + \psi_2 L_{CSC} + \psi_3 L_{CST} \quad (12)$$

## 6. Combined Loss Function

Our combined loss consists of a semantic expansion loss term and a stream re-unification loss term. For the semantic expansion loss, we combine the explicit and implicit semantic expansion losses into a single loss term we call the Semantic Expansion (SE) loss:

$$L_{SE}(\mathbf{x}) = \beta_1 L_{CE}(f_P(\mathbf{x})) + \beta_2 L_{DEX}(f_D(\mathbf{x})), \quad (13)$$

where  $f_D$  and  $f_P$  represent forward passes of data samples over the backbone, but isolated only within the implicit (DEX) and explicit (PSTE) streams respectively.  $\beta_1, \beta_2 \geq 0$  balance the mix of implicit and explicit semantic expansion. The presence of the CE loss applied on the PSTE stream acts as a counterbalance, preventing the class weight vectors from converging too closely together due to the DEX loss. Therefore, it helps in stabilizing the overall optimization objective, preventing the model from over-fitting too quickly, and restoring the representation power of the model. The hyperparameter values and relevant configurations for each stream are discussed in subsection 7.2.

**Overall Loss Function.** With the hyperparameters  $\beta_1, \beta_2, \psi_1, \psi_2, \psi_3$  controlling the relative strengths of each component loss under the hood, the overall loss function of

UDSX is presented as:

$$L_{UDSX} = L_{SE} + L_{CSR}$$

To assist in keeping track of all the components and abbreviations introduced in this work, Table 2 presents a list of abbreviations and their full form along with a short and informative description of their intended function in our proposed UDSX framework. The reader is also encouraged to look at Figure 4 as it graphically presents the relationships between all our components.

## 7. Experiments

### 7.1. Evaluation Benchmarks

#### 7.1.1. DG-ReID Datasets and Evaluation

We perform two major benchmark evaluations for DG-ReID. The traditional evaluation is conducted by training models on the combined datasets of Market-1501 [37], DukeMTMC-reID [38], CUHK02 [39], CUHK03 [40] and CUHK-SYSU [41], for a total of 121,765 images covering 18,530 person IDs. The train and test data are combined for all source datasets. The trained model is then tested on four benchmarks i-LIDS [42], PRID [43], QMUL-GRID [44] and VIPeR [45]. Due to their relatively small sizes, the test sets are shuffled in ten randomized trials and we report the mean.

M<sup>3</sup>L [1] broke from the traditional evaluation and used large-scale datasets for testing to remove uncertainty from randomized trials. In their work, the model was trained on three out of four large datasets (Market-1501, DukeMTMC-reID, CUHK03 and MSMT17\_V2 [46], which we abbreviate to M, D, C and MS respectively) and tested the model on the dataset that was left out during training. For example, C+D+MS indicates that the model was trained on a combination of CUHK03, DukeMTMC-reID and MSMT17\_V2,



**Table 2**

Abbreviation list of important components with short descriptions.

Abbrv.	Full Form	Description
DEX	Domain Embedding Expansion	Our existing implicit semantic expansion method [10]
DSD	Data Semantic Decoupling	Framework enhancement that manages implicit/explicit semantic expansion in independent streams
PSTE	Progressive Spatio-Temporal Expansion	Explicit semantic expansion applied in a controlled and localized manner. Consists of PSE and ABS
PTE	Progressive Temporal Expansion	Explicit semantic expansion applied on lower layers at start, progressing to higher layers over time
ABS	Activation-Based Stratification	Explicit semantic expansion applied only to selected strata of intermediate features, based on activation value
CSR	Contrastive-Stream Reunification	Overarching component for reunifying sibling features from implicit and explicit streams. Consists of CSP, CSC and CST
CSP	Contrastive-Stream Pairwise Loss	Feature loss ( $L_1$ ) between sibling pairs of features
CSC	Contrastive-Stream Center Loss	Modified Center Loss [35] attracting features of one stream to the centroids the other stream, and vice versa
CST	Contrastive-Stream Triplet Loss	Modified Triplet Loss [36] where anchor and positive are selected from opposing streams, while anchor and negative are from the same stream

**Table 3**

Statistics for DG-ReID datasets.

Dataset	Train		Query		Gallery	
	ID	Image	ID	Image	ID	Image
C	1367	13132	700	1400	700	5332
D	702	16522	702	2228	1110	17661
M	751	12936	750	3368	750	15913
MS	1041	32621	3060	11659	3060	82161

and therefore should be tested independently on the Market-1501 dataset. In this evaluation, only the training splits are used for training while the query/gallery split of the test dataset is used for evaluation. Four evaluations are performed, with each dataset taking turns as the target test set. Statistics of four datasets are reported in Table 3.

### 7.1.2. Image Retrieval Datasets and Evaluation

We selected a diverse range of image retrieval benchmark types to test UDSX. CUB-200-2011 (CUB) [11] consists of natural images of birds, Stanford Cars (Cars196) [12] and VehicleID [13] consist of images of cars/vehicles. Stanford Online Products [14] are images of online shopping items. Statistics for these datasets are presented in Table 4. In all datasets, training and testing classes are mutually exclusive. VehicleID provides 3 test sets, Small/Medium/Large, that contain 6493/13377/19777 images capturing 800/1600/2400 unique classes respectively. Given a test set, we randomly select an image from each class to form the probe set while the remaining images make up the gallery set, finally reporting the average Rank-1 out of 10 randomized trials. For the remaining three datasets, we follow widely used evaluation methodology [14].

## 7.2. Implementation Details

We follow the implementation described in DEX for a fair comparison. Our base model is a ResNet-50. The explicit branch uses the cross-entropy (CE) identity classification

**Table 4**

Statistics for image retrieval benchmarks.

Dataset	Classes	Images	
		Train	Test
CUB-200-2011	200	5994	5794
Stanford Cars	196	8144	8041
Stanford Online Products	22634	59551	60502
VehicleID (Full)	20207	113346	108221
VehicleID (Small)	13603	113346	6493
VehicleID (Medium)	14007	113346	13377
VehicleID (Large)	14442	113346	19777

loss. For the DEX branch, we replace the CE loss with the DEX loss as described in Equation 4. For the reunification stage, we replace the metric triplet and center losses with our own contrastive-stream reunification versions as described in subsection 7.4.4. We use a batch size of 32 which is duplicated for each of the two streams. We use a learning rate of  $\eta = 1.75e-4$ , starting at  $0.01\eta$  and linearly warming up to  $\eta$  in 10 epochs. We reduce the learning rate by a factor of 0.1 at epochs 30 and 55. We apply color jitter augmentation. For benchmarks with a large number of classes, such as the results presented in Table 6, we apply negative sampling of 2000 classes to fit the model into GPU memory [10].

For our semantic transformation policy, PSTE, we sample a Gaussian model  $\mathcal{N}$ . We apply the expansion to all intermediate layers of the backbone:  $L = [0, 1, 2, 3, 4]$ . A minimum layer width of  $\mu = 3$  layers are considered for random selection at any time. Starting with  $[0, 1, 2]$  in the first epoch, over  $T = 60$  epochs we progressively widen the set of candidate layers for selection. After  $T = 60$ , we select layers from all the layers in  $L$ .

For DSD, we use equal weights  $\beta_1 = 1$ ,  $\beta_2 = 1$  between DEX and CE losses. For CSR, we apply relative weights of  $\psi_1 = 2$ ,  $\psi_2 = 5e-4$ ,  $\psi_3 = 1$  for  $L_{CSP}$ ,  $L_{CSC}$  and  $L_{CST}$  respectively. The model trains for a total of 500 epochs.

**Table 5**

Results on the modern DG-ReID benchmarks. For the methods with the †, we evaluated the official open source implementation on this benchmark. **Bold** numbers are the best, while underlined numbers are second.

Method	Training Data	C+D+MS→M		C+M+MS→D		C+D+M→MS		D+M+MS→C		Average	
		Rank-1	mAP	Rank-1	mAP	Rank-1	mAP	Rank-1	mAP	Rank-1	mAP
QAConv [2]	Train Only	67.7	35.6	66.1	47.1	24.3	7.5	23.5	21.0	45.4	27.8
META [29] †	Train Only	66.7	44.6	61.8	42.7	32.4	13.1	21.3	21.6	45.6	30.5
OSNet-IBN [18] †	Train Only	73.4	45.1	61.5	42.3	35.7	13.7	20.9	20.9	47.9	30.5
OSNet-AIN [18] †	Train Only	74.2	47.4	62.7	44.5	37.9	14.8	22.4	22.4	49.3	32.3
DualNorm [26] †	Train Only	78.9	52.3	68.5	51.7	37.9	15.4	28.0	27.6	53.3	36.8
M <sup>3</sup> L [1]	Train Only	75.9	50.2	69.2	51.1	36.9	14.7	33.1	32.1	53.8	37.0
DEX [10]	Train Only	81.5	55.2	<u>73.7</u>	55.0	43.5	18.7	36.7	33.8	58.9	40.7
ACL [27] †	Train Only	82.8	58.4	<u>71.7</u>	53.4	<u>47.2</u>	<u>19.4</u>	35.5	34.6	<u>59.3</u>	41.5
META [29] †	Train Only	66.7	44.6	61.8	42.7	32.4	13.1	21.3	21.6	45.6	30.5
SIL [30] †	Train Only	79.2	52.8	68.3	47.0	36.9	13.8	29.5	28.9	53.5	35.6
PAT [31]	Train Only	75.2	51.7	71.8	56.5	45.6	<u>21.6</u>	31.1	31.5	55.9	40.3
CBN [47]	Train+Test	74.7	47.3	70.0	50.1	37.0	15.4	25.2	25.7	51.7	34.6
SNR [48]	Train+Test	75.2	48.5	66.7	48.3	35.1	13.8	29.1	29.0	51.5	34.9
MECL [49]	Train+Test	80.0	56.5	70.0	53.4	32.7	13.3	32.1	31.5	53.7	38.7
RaMoE [28]	Train+Test	82.0	56.5	73.6	<b>56.9</b>	34.1	13.5	36.6	35.5	56.6	40.6
MixNorm [50]	Train+Test	78.9	51.4	70.8	49.9	<u>47.2</u>	<u>19.4</u>	29.6	29.0	56.6	37.4
MetaBIN [51]	Train+Test	<u>83.2</u>	<b>61.2</b>	71.3	54.9	40.8	17.0	<u>38.1</u>	<b>37.5</b>	58.4	<u>42.7</u>
<b>UDSX (Ours)</b>	Train Only	<b>85.7</b>	<u>60.4</u>	<b>74.7</b>	<u>55.8</u>	<b>47.6</b>	<b>20.2</b>	<b>38.9</b>	<u>37.2</u>	<b>61.7</b>	<b>43.4</b>

**Table 6**

Results on the traditional DG-ReID setting. To save space, methods are cited in 7.3.1

Method	R-1	R-5	mAP	R-1	R-5	mAP
	GRID			i-LIDS		
AugMining	46.6	67.5	-	76.3	93.0	-
DIR-ReID	47.8	51.1	52.1	74.4	83.1	78.6
RaMoE	46.8	-	54.2	85.0	-	90.2
SNR	40.2	-	47.7	84.1	-	89.9
DTIN-Net	51.8	-	60.6	81.8	-	87.2
MetaBIN	48.4	-	57.9	81.3	-	87.0
BCaR	52.8	-	-	81.3	-	-
DEX	53.3	69.4	61.7	86.3	95.2	90.7
<b>UDSX</b>	<b>56.9</b>	<b>72.7</b>	<b>63.0</b>	<b>86.7</b>	<b>98.0</b>	<b>91.4</b>
	PRID			VIPeR		
AugMining	34.3	56.2	-	49.8	70.8	-
DIR-ReID	71.1	82.4	75.6	58.3	66.9	62.9
RaMoE	57.7	-	67.3	56.6	-	64.6
SNR	52.1	-	66.5	52.9	-	61.3
DTIN-Net	71.0	-	79.7	62.9	-	70.7
MetaBIN	74.2	-	81.0	59.9	-	68.6
BCaR	70.2	-	-	65.8	-	-
DEX	71.0	87.8	78.5	65.5	79.2	72.0
<b>UDSX</b>	<b>77.6</b>	<b>90.5</b>	<b>83.1</b>	<b>66.1</b>	<b>83.2</b>	<b>73.5</b>

During inference, DEX and PSTE are disabled and the inputs feed forward through the backbone without semantic expansion.

### 7.3. SOTA Methods Comparison

#### 7.3.1. DG-ReID Task

UDSX outperforms or matches current SOTA methods in all standard evaluations for DG-ReID. Table 5 compares UDSX with the recent strongest performing SOTA methods in the modern evaluation, which was established by M<sup>3</sup>L [1]. As a test of UDSX’s ability, we included results from other

methods that tested on a closely-related benchmark where training and testing sets are merged together within the source domains to get more training data, while the target test domain remains the same. Even with the significant handicap of using less training data, our method is still able to surpass the performance of the methods using more data for a majority of the benchmarks, showing that UDSX learns more efficiently from data than its competitors. If we restrict to only the same training-set-only benchmark, our method surpasses the SOTA in all evaluations by a significant margin. Furthermore, considering the average Rank-1 and mAP performance across all four target domains, our method still emerges on top regardless of amount of source training data, demonstrating the superior all-round performance of UDSX.

Table 6 presents UDSX for the traditional evaluation methodology, again comparing with the strongest in the field such as AugMining [52], DIR-ReID [53], RaMoE [28], SNR [48], DTIN-Net [54], MetaBIN [51] and BCaR [55]. In the modern evaluation, UDSX surpasses the SOTA performance for all four benchmarks. Notably, UDSX’s performance on C+D+MS → M pushed the SOTA by more than 2% in Rank-1 and mAP and for C+D+M → MS by more than 4% in Rank-1. In both modern and traditional DG-ReID benchmarks, UDSX emerges in the first place and demonstrates the effectiveness of combining explicit and implicit semantic expansion methods in the task of DG-ReID.

#### 7.3.2. Image Retrieval Tasks

Table 7 compares UDSX against other recent SOTA methods in image retrieval. For fairness, we compare methods that all use a ResNet-50 backbone, such as NormSoftMax [56], MS512 [57], ROADMAP [58], ProxyNCA++ [59], AVSL [60], Metrix [61], SCT [62], Recall@k Surrogate Loss [63], VehicleNet [64], Smooth-AP

**Table 7**

Results on general image retrieval benchmarks. To save space, methods are cited in 7.3.2

Method	Rank-1	Method	Rank-1		
CUB-200-2011		Stanford Cars (Cars196)			
NormSoftMax	65.3	MS512	84.1		
MS512	65.7	NormSoftmax	89.3		
ROADMAP	68.5	ProxyNCA++	90.1		
ProxyNCA++	72.2	AVSL	91.5		
ISDA	73.4	ISDA	90.9		
DEX	75.4	DEX	91.2		
<b>UDSX</b>	<b>77.8</b>	<b>UDSX</b>	<b>92.6</b>		
Stanford Online Products		VehicleID			
			<u>Small</u>	<u>Medium</u>	<u>Large</u>
Metrix	81.3	VehicleNet	83.6	81.4	79.5
SCT	81.6	Smooth-AP	94.9	93.3	91.9
Recall@K	82.7	RPTM	95.1	93.3	92.7
ROADMAP	83.1	Recall@K	95.7	94.6	93.8
ISDA	83.4	ISDA	94.7	93.2	92.8
DEX	83.5	DEX	94.2	94.2	92.2
<b>UDSX</b>	<b>85.0</b>	<b>UDSX</b>	<b>96.8</b>	<b>95.0</b>	<b>94.7</b>

Loss [65] and RPTM [66]. For completeness, we also compare with implicit semantic expansion techniques ISDA [5] and DEX [10]. In all of these benchmarks, UDSX achieves the best Rank-1 score, demonstrating that our design improves implicit semantic expansion methods and allows for better performance not only in Person ReID but also in the image retrieval field at large.

## 7.4. Ablation Studies

### 7.4.1. Components of UDSX

Table 8 presents an ablation study of the influence due to the components of UDSX. The study is performed on two DG-ReID benchmarks ( $C+D+MS \rightarrow M$  and  $C+D+M \rightarrow MS$ ) and one general image retrieval benchmark (CUB-200-2011). The first two configurations, PSTE/DEX Only, do not require duplicate data streams, meaning that DSD is switched off. In PSTE Only, we perform explicit semantic expansion following the scheme described in subsection 4.2.2 and use the standard cross-entropy, center and triplet losses while leaving out DEX and CSR. Similarly, in DEX Only we train only with the DEX loss and omit everything else. DEX+Naive performs explicit semantic expansion on a single stream of features while also applying the DEX loss. It demonstrates that naively combining them leads to poor results. For the rest of the configurations, we cumulatively add components of UDSX to DEX, starting with Data Semantic Decoupling (DEX + DSD), followed by Progressive Spatio-Temporal Expansion (DEX + DSD + PSTE) and finally add Contrastive-Stream Reunification to get our full method, UDSX. Our experiments demonstrate that each component improves generalization scores in DG-ReID and also in image retrieval. Furthermore, we observe that using PSTE Only surpasses DEX Only in some benchmarks like  $C+D+MS \rightarrow M$  and CUB-200-2011, but their combined strengths yield the best results.

### 7.4.2. Hyperparameter Study

Our method UDSX employs five important parameters that belong in two groups. The first group,  $\beta_1$  and  $\beta_2$ , control

**Table 8**

Ablation over configurations of UDSX. For PSTE/DEX Only, we only use a single data stream and train with the respective loss. Only configurations with DSD require two data streams.

Benchmark	Configuration	Rank-1	mAP
$C+D+MS \rightarrow M$	PSTE Only	81.8	55.5
	DEX Only	80.0	55.1
	DEX + Naive	79.8	53.6
	DEX + DSD	84.0	58.2
	DEX + DSD + PSTE	84.8	58.4
	<b>UDSX (Ours)</b>	<b>85.7</b>	<b>60.4</b>
$C+D+M \rightarrow MS$	PSTE Only	40.9	16.5
	DEX Only	43.0	18.3
	DEX + Naive	43.2	18.2
	DEX + DSD	44.4	19.1
	DEX + DSD + PSTE	45.7	19.4
	<b>UDSX (Ours)</b>	<b>47.6</b>	<b>20.2</b>
CUB-200-2011	PSTE Only	74.2	61.9
	DEX Only	75.8	60.9
	DEX + Naive	75.4	54.7
	DEX + DSD	76.5	62.5
	DEX + DSD + PSTE	77.1	63.1
	<b>UDSX (Ours)</b>	<b>77.6</b>	<b>63.6</b>

the strengths of explicit and implicit semantic expansion, while the second group,  $\psi_1$ ,  $\psi_2$  and  $\psi_3$ , balance the components in the reunification process of Contrastive-Stream Reunification. We investigate the effects of these two groups of hyperparameters in each of the following sub-sections, using the same two multi-source DG-ReID benchmarks,  $C+D+MS \rightarrow M$  and  $C+D+M \rightarrow MS$ .

### 7.4.3. Explicit/Implicit Trade-off

Table 9 compares the effects of varying the relative strengths between explicit ( $\beta_1$ ) and implicit ( $\beta_2$ ) semantic expansion. Starting with  $\beta_1 = 1, \beta_2 = 0$ , we increase the strength of DEX via  $\beta_2$  until they are evenly matched at  $\beta_1 = 1, \beta_2 = 1$ . We do this in the opposite direction as well, starting from  $\beta_1 = 0, \beta_2 = 1$  and increasing  $\beta_1$  until we reach  $\beta_1 = 1, \beta_2 = 1$ . First, we can observe that when operating individually without the other, implicit semantic expansion is stronger than the explicit by a few percentage points in Rank-1 and mAP for both benchmarks. Furthermore, even with a relatively low implicit semantic expansion weight ( $\beta_2$ ), the performance of our UDSX already increases significantly. However, we also observe that further increasing  $\beta_2$  beyond this low weight does not improve performance much. Instead, while explicit semantic expansion alone is comparatively less effective, it plays a strong supporting role by boosting the performance beyond the limitations imposed by the implicit semantic expansion, as discussed in subsection 3.2. This comparison experimentally justifies our intention to supplement DEX with explicit semantic expansion to help overcome its limits.

### 7.4.4. CSR Components Analysis

We study the effects of the three components of CSR, as shown in Table 10. For the CSP loss study, we compare

**Table 9**

Varying the strengths between explicit (PSTE) and implicit (DEX) semantic expansion, both of which are controlled by hyperparameters  $\beta_1$  and  $\beta_2$  respectively (See Eq. 13).

Benchmark	$\beta_1$	$\beta_2$	Rank-1	mAP
C+D+MS $\rightarrow$ M	1.0	0.0	81.7	54.1
	1.0	0.4	84.9	59.9
	1.0	0.8	85.1	59.9
	1.0	1.0	<b>85.7</b>	<b>60.4</b>
	0.8	1.0	85.6	60.1
	0.4	1.0	85.0	59.6
	0.0	1.0	83.0	56.5
C+D+M $\rightarrow$ MS	1.0	0.0	41.1	16.7
	1.0	0.4	44.8	18.9
	1.0	0.8	45.6	19.2
	1.0	1.0	<b>47.6</b>	<b>20.2</b>
	0.8	1.0	45.9	19.6
	0.4	1.0	45.0	19.1
	0.0	1.0	45.0	19.0

**Table 10**

Ablation study over components of the contrastive stream losses in CSR (See Eq. 12).

Benchmark	Config	Rank-1	mAP
C+D+MS $\rightarrow$ M	Baseline	81.7	54.7
	CSP ( $\psi_1 = 1$ )	<b>85.4</b>	<b>59.0</b>
	CSP ( $\psi_1 = 2$ )	84.9	59.0
	CSP ( $\psi_1 = 5$ )	85.1	58.9
	Center ( $\psi_2 = 5e-4$ )	80.8	54.0
	CSC ( $\psi_2 = 5e-4$ )	<b>84.3</b>	<b>57.8</b>
	Triplet ( $\psi_3 = 1$ )	81.9	55.8
	CST ( $\psi_3 = 1$ )	<b>85.1</b>	<b>57.9</b>
C+D+M $\rightarrow$ MS	Baseline	43.3	17.9
	CSP ( $\psi_1 = 1$ )	<b>43.7</b>	<b>18.4</b>
	CSP ( $\psi_1 = 2$ )	42.9	17.7
	CSP ( $\psi_1 = 5$ )	42.3	17.7
	Center ( $\psi_2 = 5e-4$ )	43.4	18.7
	CSC ( $\psi_2 = 5e-4$ )	<b>45.9</b>	<b>19.0</b>
	Triplet ( $\psi_3 = 1$ )	43.0	18.0
	CST ( $\psi_3 = 1$ )	<b>43.6</b>	<b>18.5</b>

a baseline without CSP Loss against three other models trained on CSC loss with weights  $\psi_1 \in \{1, 2, 5\}$ . CSC and CST are compared against the standard Center [35] and Triplet [36] losses respectively with the same weight. For CSC/Center loss, the standard weight is  $\psi_2 = 5e-4$  and for CST/Triplet loss it is  $\psi_3 = 1$ . Our experiment shows that for CSP loss, a moderate weight of  $\psi_1 = 1$  improves results. Also, we found that replacing the standard Center and Triplet losses with our CSC and CST losses improves results significantly. These experiments show that the Contrastive-Stream Pairwise Loss is an effective stream unifier and the other components of Contrastive-Stream Reunification are more effective over the standard Center and Triplet losses.

**Table 11**

Varying strength of DEX via  $\lambda$  on all four major DG-ReID benchmarks. Values in parentheses are for DEX only with no explicit expansion. Through this study, we demonstrate that our design choices in UDSX mitigate early over-fitting and can accommodate stronger DEX weights.

Benchmark	$\lambda$	Best Epoch	mAP	Rank-1
C+D+MS $\rightarrow$ M	No DEX ( $\lambda = 0$ )	307 (57)	55.1 (54.0)	82.1 (79.8)
	5	310 (39)	59.2 (54.8)	85.1 (81.1)
	15	322 (39)	<b>60.4</b> (54.2)	<b>85.7</b> (80.2)
	25	322 (35)	59.7 (54.1)	85.0 (79.7)
	50	112 (34)	59.3 (52.7)	84.7 (78.1)
C+D+M $\rightarrow$ MS	No DEX ( $\lambda = 0$ )	68 (201)	16.5 (18.3)	40.9 (43.4)
	5	156 (99)	19.3 (18.6)	45.4 (43.9)
	15	198 (99)	<b>20.2</b> (19.1)	<b>47.6</b> (44.8)
	25	198 (114)	19.3 (18.5)	45.8 (43.0)
	50	60 (45)	19.0 (18.5)	44.6 (43.3)
C+M+MS $\rightarrow$ D	No DEX ( $\lambda = 0$ )	391 (252)	53.8 (54.1)	72.3 (72.6)
	5	382 (105)	54.0 (54.6)	72.1 (72.3)
	15	287 (78)	<b>55.8</b> (54.9)	<b>74.7</b> (73.5)
	25	238 (72)	55.0 (54.0)	73.8 (73.0)
	50	307 (42)	54.9 (53.7)	73.1 (72.5)
D+M+MS $\rightarrow$ C	No DEX ( $\lambda = 0$ )	492 (111)	34.2 (29.3)	35.2 (29.5)
	5	357 (120)	34.7 (30.4)	36.2 (31.6)
	15	207 (108)	<b>37.2</b> (33.2)	<b>38.9</b> (34.1)
	25	265 (114)	36.5 (33.8)	37.1 (35.4)
	50	137 (78)	35.2 (33.5)	35.4 (35.1)

#### 7.4.5. Robustness to Over-Fitting

Table 11 demonstrates that UDSX is able to achieve good results under stronger application of DEX, which is controlled by  $\lambda$ . We compared UDSX against DEX across the four major DG-ReID benchmarks and across values of  $\lambda \in \{5, 15, 25, 50\}$ . Results for UDSX are presented first while results for DEX are in parentheses. Across the board, the addition of explicit semantic expansion is shown to yield a net positive benefit. Compared with DEX alone, we can see that the epoch at which model performance peaks (Best Epoch) is significantly higher for UDSX. In C+D+MS  $\rightarrow$  M and D+M+MS  $\rightarrow$  C, the application of explicit semantic expansion shows a clear and significant performance improvement, while in C+D+M  $\rightarrow$  MS explicit expansion improves Rank-1 by a wide margin. In these benchmarks, we demonstrate that UDSX mitigates the degradation of performance caused by over-fitting, allowing the model to train effectively for more epochs and reach better evaluation scores than before.

## 8. Conclusion

Implicit semantic expansion methods, while powerful, have inherent drawbacks that limit its generalization capacity when learning from datasets with a large number of classes. Naively combining implicit and explicit semantic expansion is generally detrimental and requires finesse in order to get them to work together. In this work, we unified both of them in a single framework, UDSX, such that the strengths of both types of semantic expansion are synergized, and achieve new state-of-the-art results in DG-ReID and general image retrieval benchmarks.

## Acknowledgement

This work was supported by the Defence Science and Technology Agency (DSTA) Postgraduate Scholarship, of which Eugene P.W. Ang is a recipient. It was carried out at the Rapid-Rich Object Search (ROSE) Lab at the Nanyang Technological University, Singapore.

## CRedit authorship contribution statement

**Eugene P.W. Ang:** Conceptualization; Formal analysis; Investigation; Methodology; Software; Validation; Visualization; Roles/Writing - original draft; Writing - review & editing. **Shan Lin:** Methodology; Project administration; Resources; Supervision; Writing - review & editing. **Alex C. Kot:** Project administration; Resources; Supervision; Writing - review & editing.

## Declaration of competing interest

The authors declare that they have no known competing financial interests or personal relationships that could have appeared to influence the work reported in this paper.

## Data availability

Data will be made available on request.

## References

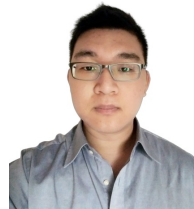
- [1] Y. Zhao, Z. Zhong, F. Yang, Z. Luo, Y. Lin, S. Li, N. Sebe, Learning to Generalize Unseen Domains via Memory-based Multi-Source Meta-Learning for Person Re-Identification, in: Proceedings of the IEEE/CVF Conference on Computer Vision and Pattern Recognition (CVPR), 2020, pp. 6277–6286. [arXiv:2012.00417](https://arxiv.org/abs/2012.00417).
- [2] S. Liao, L. Shao, Interpretable and Generalizable Deep Image Matching with Adaptive Convolutions, European Conference on Computer Vision (ECCV) abs/1904.1 (2020).
- [3] J. Song, Y. Yang, Y. Z. Song, T. Xiang, T. M. Hospedales, Generalizable person re-identification by domain-invariant mapping network, in: Proceedings of the IEEE Computer Society Conference on Computer Vision and Pattern Recognition, volume 2019-June, 2019, pp. 719–728.
- [4] Y. Wang, G. Huang, S. Song, X. Pan, Y. Xia, C. Wu, Regularizing Deep Networks with Semantic Data Augmentation, IEEE Transactions on Pattern Analysis and Machine Intelligence (2021) 1.
- [5] Y. Wang, X. Pan, S. Song, H. Zhang, C. Wu, G. Huang, Implicit semantic data augmentation for deep networks, in: Advances in Neural Information Processing Systems, volume 32, 2019. [arXiv:1909.12220](https://arxiv.org/abs/1909.12220).
- [6] H. Noh, T. You, J. Mun, B. Han, Regularizing Deep Neural Networks by Noise: Its Interpretation and Optimization, in: I. Guyon, U. V. Luxburg, S. Bengio, H. Wallach, R. Fergus, S. Vishwanathan, R. Garnett (Eds.), Advances in Neural Information Processing Systems, volume 30, Curran Associates, Inc., 2017.
- [7] Z. He, A. S. Rakin, D. Fan, Parametric noise injection: Trainable randomness to improve deep neural network robustness against adversarial attack, in: Proceedings of the IEEE Conference on Computer Vision and Pattern Recognition, 2019, pp. 588–597.
- [8] S. H. Lim, N. B. Erichson, F. Utrera, W. Xu, M. W. Mahoney, Noisy Feature Mixup, [ArXiv abs/2110.0](https://arxiv.org/abs/2110.0) (2022).
- [9] K. He, X. Zhang, S. Ren, J. Sun, Deep residual learning for image recognition, in: Proceedings of the IEEE Computer Society Conference on Computer Vision and Pattern Recognition, volume 2016-December, 2016, pp. 770–778. [arXiv:1512.03385](https://arxiv.org/abs/1512.03385).
- [10] E. Ang, S. Lin, A. C. Kot, DEX: Domain Embedding Expansion for Generalized Person Re-identification, in: The 32nd British Machine Vision Conference, 2021, p. 14.
- [11] C. Wah, S. Branson, P. Welinder, P. Perona, S. Belongie, Caltech-UCSD Birds-200-2011, Technical Report, Caltech Vision Lab, 2011.
- [12] J. Krause, M. Stark, J. Deng, L. Fei-Fei, 3D Object Representations for Fine-Grained Categorization, in: 4th International IEEE Workshop on 3D Representation and Recognition (3dRR-13), Sydney, Australia, 2013.
- [13] H. Liu, Y. Tian, Y. Wang, L. Pang, T. Huang, Deep Relative Distance Learning: Tell the Difference Between Similar Vehicles, in: Proceedings of the IEEE Conference on Computer Vision and Pattern Recognition, 2016, pp. 2167–2175.
- [14] H. O. Song, Y. Xiang, S. Jegelka, S. Savarese, Deep Metric Learning via Lifted Structured Feature Embedding, in: Computer Vision and Pattern Recognition (CVPR), 2016.
- [15] Y. Sun, L. Zheng, Y. Yang, Q. Tian, S. Wang, Beyond part models: Person retrieval with refined part pooling (and a strong convolutional baseline), [arXiv \(2017\)](https://arxiv.org/abs/1707.07501).
- [16] H. Luo, Y. Gu, X. Liao, S. Lai, W. Jiang, Bag of tricks and a strong baseline for deep person re-identification, in: IEEE Computer Society Conference on Computer Vision and Pattern Recognition Workshops, volume 2019-June, 2019, pp. 1487–1495. [arXiv:1903.07071](https://arxiv.org/abs/1903.07071).
- [17] G. Wang, Y. Yuan, X. Chen, J. Li, X. Zhou, Learning discriminative features with multiple granularities for person re-identification, in: MM 2018 - Proceedings of the 2018 ACM Multimedia Conference, 2018, pp. 274–282. doi:10.1145/3240508.3240552. [arXiv:1804.01438](https://arxiv.org/abs/1804.01438).
- [18] K. Zhou, Y. Yang, A. Cavallaro, T. Xiang, Learning Generalisable Omni-Scale Representations for Person Re-Identification, in: IEEE Transactions on Pattern Analysis and Machine Intelligence, 2021. doi:10.1109/TPAMI.2021.3069237. [arXiv:1910.06827](https://arxiv.org/abs/1910.06827).
- [19] W. Deng, L. Zheng, Q. Ye, G. Kang, Y. Yang, J. Jiao, Image-Image Domain Adaptation with Preserved Self-Similarity and Domain-Dissimilarity for Person Re-identification, in: Proceedings of the IEEE Computer Society Conference on Computer Vision and Pattern Recognition, 2018, pp. 994–1003. [arXiv:1711.07027](https://arxiv.org/abs/1711.07027).
- [20] S. Lin, H. Li, C. T. Li, A. C. Kot, Multi-task mid-level feature alignment network for unsupervised cross-dataset person re-identification, in: British Machine Vision Conference 2018, BMVC 2018, 2019. [arXiv:1807.01440](https://arxiv.org/abs/1807.01440).
- [21] S. Lin, C.-T. Li, A. C. Kot, Multi-Domain Adversarial Feature Generalization for Person Re-Identification, IEEE Transactions on Image Processing (2020).
- [22] J. Wang, X. Zhu, S. Gong, W. Li, Transferable Joint Attribute-Identity Deep Learning for Unsupervised Person Re-identification, in: Proceedings of the IEEE Computer Society Conference on Computer Vision and Pattern Recognition, 2018, pp. 2275–2284. doi:10.1109/CVPR.2018.00242. [arXiv:1803.09786](https://arxiv.org/abs/1803.09786).
- [23] Y. Dai, J. Liu, Y. Sun, Z. Tong, C. Zhang, L.-Y. Duan, IDM: An Intermediate Domain Module for Domain Adaptive Person Re-ID, in: Proceedings of the IEEE/CVF International Conference on Computer Vision, 2021.
- [24] K. Zheng, W. Liu, L. He, T. Mei, J. Luo, Z.-J. Zha, Group-aware label transfer for domain adaptive person re-identification, in: Proceedings of the IEEE/CVF Conference on Computer Vision and Pattern Recognition, 2021, pp. 5310–5319.
- [25] K. Zheng, C. Lan, W. Zeng, Z. Zhang, Z.-J. Zha, Exploiting Sample Uncertainty for Domain Adaptive Person Re-Identification, in: Proceedings of the AAAI Conference on Artificial Intelligence, volume 35, 2021, pp. 3538–3546.
- [26] J. Jia, Q. Ruan, T. M. Hospedales, Frustratingly easy person re-identification: Generalizing person Re-ID in practice, in: 30th British Machine Vision Conference 2019, BMVC 2019, 2020. [arXiv:1905.03422](https://arxiv.org/abs/1905.03422).
- [27] P. Zhang, H. Dou, Y. Yu, X. Li, Adaptive cross-domain learning for generalizable person re-identification, in: S. Avidan, G. Brostow, M. Cissé, G. M. Farinella, T. Hassner (Eds.), Computer Vision – ECCV 2022, Springer Nature Switzerland, Cham, 2022, pp. 215–232.

- [28] Y. Dai, X. Li, J. Liu, Z. Tong, L.-Y. Duan, Generalizable Person Re-identification with Relevance-aware Mixture of Experts, in: 2021 Conference on Computer Vision and Pattern Recognition (CVPR), 2021. [arXiv:2105.09156](https://arxiv.org/abs/2105.09156).
- [29] B. Xu, J. Liang, L. He, Z. Sun, Mimic embedding via adaptive aggregation: Learning generalizable person re-identification, in: S. Avidan, G. Brostow, M. Cissé, G. M. Farinella, T. Hassner (Eds.), *Computer Vision – ECCV 2022*, Springer Nature Switzerland, Cham, 2022, pp. 372–388.
- [30] W. Tan, C. Ding, P. Wang, M. Gong, K. Jia, Style interleaved learning for generalizable person re-identification, *IEEE Transactions on Multimedia* (2023).
- [31] H. Ni, Y. Li, L. Gao, H. T. Shen, J. Song, Part-aware transformer for generalizable person re-identification, in: *Proceedings of the IEEE/CVF International Conference on Computer Vision*, 2023, pp. 11280–11289.
- [32] D. Hendrycks, S. Basart, N. Mu, S. Kadavath, F. Wang, E. Dorundo, R. Desai, T. Zhu, S. Parajuli, M. Guo, D. Song, J. Steinhart, J. Gilmer, The many faces of robustness: A critical analysis of out-of-distribution generalization, *ICCV* (2021).
- [33] P. Upchurch, J. Gardner, G. Pleiss, R. Pless, N. Snavely, K. Bala, K. Q. Weinberger, Deep Feature Interpolation For Image Content Changes, in: *The IEEE Conference on Computer Vision and Pattern Recognition (CVPR)*, 2017.
- [34] D. Wu, S.-T. Xia, Y. Wang, Adversarial weight perturbation helps robust generalization, in: *NeurIPS*, 2020.
- [35] Y. Wen, K. Zhang, Z. Li, Y. Qiao, A Discriminative Feature Learning Approach for Deep Face Recognition, in: *Proc. European Conference on Computer Vision (ECCV)*, volume 9911 LNCS, Springer Science+Business Media, 2016, pp. 499–515.
- [36] A. Hermans, L. Beyer, B. Leibe, In Defense of the Triplet Loss for Person Re-Identification, in: *arXiv preprint*, 2017. [arXiv:1703.07737](https://arxiv.org/abs/1703.07737).
- [37] L. Zheng, L. Shen, L. Tian, S. Wang, J. Wang, Q. Tian, Scalable person re-identification: A benchmark, in: *Proceedings of the IEEE International Conference on Computer Vision*, volume 2015 Inter, 2015, pp. 1116–1124.
- [38] Z. Zheng, L. Zheng, Y. Yang, Unlabeled Samples Generated by GAN Improve the Person Re-identification Baseline in Vitro, in: *Proceedings of the IEEE International Conference on Computer Vision*, volume 2017-October, 2017, pp. 3774–3782. [arXiv:1701.07717](https://arxiv.org/abs/1701.07717).
- [39] W. Li, X. Wang, Locally aligned feature transforms across views, in: *Proceedings of the IEEE Computer Society Conference on Computer Vision and Pattern Recognition*, 2013, pp. 3594–3601.
- [40] W. Li, R. Zhao, T. Xiao, X. Wang, DeepReID: Deep Filter Pairing Neural Network for Person Re-identification, in: *2014 IEEE Conference on Computer Vision and Pattern Recognition*, 2014, pp. 152–159.
- [41] S. Qiao, C. Liu, W. Shen, A. Yuille, Few-Shot Image Recognition by Predicting Parameters from Activations, in: *Proceedings of the IEEE Computer Society Conference on Computer Vision and Pattern Recognition*, 2018, pp. 7229–7238. [arXiv:1706.03466](https://arxiv.org/abs/1706.03466).
- [42] W. S. Zheng, S. Gong, T. Xiang, Associating groups of people, in: *British Machine Vision Conference, BMVC 2009 - Proceedings*, 2009, pp. 21–23.
- [43] M. Hirzer, C. Beleznaï, P. M. Roth, H. Bischof, Person re-identification by descriptive and discriminative classification, in: *Lecture Notes in Computer Science (including subseries Lecture Notes in Artificial Intelligence and Lecture Notes in Bioinformatics)*, volume 6688 LNCS, 2011, pp. 91–102.
- [44] C. C. Loy, T. Xiang, S. Gong, Multi-camera activity correlation analysis, in: *2009 IEEE Computer Society Conference on Computer Vision and Pattern Recognition Workshops, CVPR Workshops 2009*, volume 2009 IEEE, 2009, pp. 1988–1995.
- [45] D. Gray, S. Brennan, H. Tao, Evaluating appearance models for recognition, reacquisition, and tracking, in: *10th International Workshop on Performance Evaluation for Tracking and Surveillance (PETS)*, volume 3, 2007, pp. 41–47.
- [46] L. Wei, S. Zhang, W. Gao, Q. Tian, Person Transfer GAN to Bridge Domain Gap for Person Re-identification, in: *Proceedings of the IEEE Computer Society Conference on Computer Vision and Pattern Recognition*, 2018, pp. 79–88. doi:10.1109/CVPR.2018.00016. [arXiv:1711.08565](https://arxiv.org/abs/1711.08565).
- [47] Z. Zhuang, L. Wei, L. Xie, T. Zhang, H. Zhang, H. Wu, H. Ai, Q. Tian, Rethinking the distribution gap of person re-identification with camera-based batch normalization, in: *European Conference on Computer Vision*, Springer, 2020, pp. 140–157.
- [48] X. Jin, C. Lan, W. Zeng, Z. Chen, L. Zhang, Style Normalization and Restitution for Generalizable Person Re-Identification, in: *Proceedings of the IEEE Computer Society Conference on Computer Vision and Pattern Recognition*, 2020, pp. 3140–3149. [arXiv:2005.11037](https://arxiv.org/abs/2005.11037).
- [49] S. Yu, F. Zhu, D. Chen, R. Zhao, H. Chen, S. Tang, J. Zhu, Y. Qiao, Multiple domain experts collaborative learning: Multi-source domain generalization for person re-identification, 2021. [arXiv:2105.12355](https://arxiv.org/abs/2105.12355).
- [50] L. Qi, L. Wang, Y. Shi, X. Geng, A novel mix-normalization method for generalizable multi-source person re-identification, *IEEE Transactions on Multimedia* (2022) 1–12.
- [51] S. Choi, T. Kim, M. Jeong, H. Park, C. Kim, Meta Batch-Instance Normalization for Generalizable Person Re-Identification, in: *Proceedings of the IEEE/CVF Conference on Computer Vision and Pattern Recognition (CVPR)*, 2021.
- [52] M. Tamura, T. Murakami, Augmented Hard Example Mining for Generalizable Person Re-Identification, in: *arXiv preprint*, 2019. [arXiv:1910.05280](https://arxiv.org/abs/1910.05280).
- [53] Y.-F. Zhang, H. Zhang, Z. Zhang, D. Li, Z. Jia, L. Wang, T. Tan, Learning Domain Invariant Representations for Generalizable Person Re-Identification, *CoRR abs/2103.1* (2021).
- [54] B. Jiao, L. Liu, L. Gao, G. Lin, L. Yang, S. Zhang, P. Wang, Y. Zhang, Dynamically Transformed Instance Normalization Network for Generalizable Person Re-Identification, in: *European Conference on Computer Vision*, Springer Science+Business Media, 2022.
- [55] M. Tamura, T. Yoshinaga, BCaR: Beginner Classifier as Regularization Towards Generalizable Re-ID, in: *BMVC*, 2020.
- [56] A. Zhai, H.-Y. Wu, Classification is a Strong Baseline for Deep Metric Learning, in: *30th British Machine Vision Conference 2019, BMVC 2019, The British Machine Vision Association and Society for Pattern Recognition*, 2019, p. 12.
- [57] X. Wang, X. Han, W. Huang, D. Dong, M. R. Scott, Multi-Similarity Loss with General Pair Weighting for Deep Metric Learning, in: *Proceedings of the IEEE Conference on Computer Vision and Pattern Recognition*, 2019, pp. 5022–5030.
- [58] E. Ramzi, N. THOME, C. Rambour, N. Audebert, X. Bitot, Robust and Decomposable Average Precision for Image Retrieval, in: *Thirty-Fifth Conference on Neural Information Processing Systems*, 2021.
- [59] G. W. T. Eu Wern Teh, Terrance DeVries, ProxyNCA++: Revisiting and Revitalizing Proxy Neighborhood Component Analysis, in: *European Conference on Computer Vision (ECCV)*, Springer Science+Business Media, 2020, p. 17.
- [60] B. Zhang, W. Zheng, J. Zhou, J. Lu, Attributable Visual Similarity Learning, in: *Proceedings of the IEEE Conference on Computer Vision and Pattern Recognition*, 2022.
- [61] E. K. L. A. K. K. Y. A. Shashanka Venkataramanan Bill Psomas, It Takes Two to Tango: Mixup for Deep Metric Learning, in: *The Tenth International Conference on Learning Representations*, 2022.
- [62] H. Xuan, A. Stylianou, X. Liu, R. Pless, Hard negative examples are hard, but useful, in: *European Conference on Computer Vision*, Springer, 2020, pp. 126–142.
- [63] Y. Patel, G. Tolia, J. Matas, Recall@k Surrogate Loss with Large Batches and Similarity Mixup, in: *Proceedings of the IEEE/CVF Conference on Computer Vision and Pattern Recognition*, 2022, pp. 7492–7501.
- [64] Z. Zheng, T. Ruan, Y. Wei, Y. Yang, VehicleNet: Learning Robust Feature Representation for Vehicle Re-identification, in: *Proceedings of the IEEE/CVF Conference on Computer Vision and Pattern Recognition (CVPR) Workshops*, 2019.

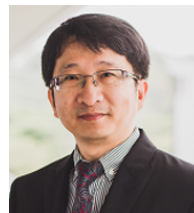
- [65] A. Brown, W. Xie, V. Kalogeiton, A. Zisserman, Smooth-AP: Smoothing the Path Towards Large-Scale Image Retrieval, in: European Conference on Computer Vision (ECCV), 2020., 2020.
- [66] W.-Y. L. Adhiraj Ghosh Kuruparan Shanmugalingam, Relation Preserving Triplet Mining for Stabilizing the Triplet Loss in Vehicle Re-identification, arXiv preprint (2021).



Eugene P.W. Ang received both the B.Sc. in Computer Science in 2007 and M.Sc. in Information Systems Management in 2008 from Carnegie Mellon University, USA. He also received the M.Sc. in Computer Science (Machine Learning Track) from Columbia University, USA, in 2017. Under a post-graduate scholarship from the Defence Science and Technology Agency he is currently a PhD candidate in ROSE Lab, Nanyang Technological University, Singapore, where he pursues research on the practical applications of deep learning and computer vision such as domain generalized person/object re-identification and has published several papers in these areas.



Shan Lin received the B.Sc. degree and Ph.D. degree from the University of Warwick, U.K, in 2015 and 2020. He is currently a research fellow in ROSE Lab, Nanyang Technological University, Singapore. His current research interests are in the area of person re-identification, computer vision, and deep learning. His studies are funded by the European Union EU H2020 project IDENTITY and National Research Foundation, Singapore under AI Singapore program. He has published several technical papers in these areas.



Prof. Alex C. Kot has been with the Nanyang Technological University (NTU), Singapore since 1991. He headed the Division of Information Engineering at the School of Electrical and Electronic Engineering (EEE) for eight years. He was the Vice Dean Research and Associate Chair (Research) for the School of EEE for three years, overseeing the research activities for the School with over 200 faculty members. He was the Associate Dean (Graduate Studies) for the College of Engineering (COE) for eight years. He is currently the Director of ROSE Lab [Rapid(Rich) Object SEarch Lab] and the Director of NTU-PKU Joint Research Institute. He has published extensively with over 300 technical papers in the areas of signal processing for communication, biometrics recognition, authentication, image forensics, machine learning and AI. Prof. Kot served as Associate Editor for a number of IEEE transactions, including IEEE TSP, IMM, TCSVT, TCAS-I, TCAS-II, TIP, SPM, SPL, JSTSP, JASP, TIFS, etc. He was a TC member for several IEEE Technical Committee in SPS and CASS. He has served the IEEE in various capacities such as the General Co-Chair for the 2004 IEEE International Conference on Image Processing (ICIP) and area/track chairs for several IEEE flagship conferences. He also served as the IEEE Signal Processing Society Distinguished Lecturer Program Coordinator and the Chapters Chair for IEEE Signal Processing Chapters worldwide. He received the Best Teacher of The Year Award at NTU, the Microsoft MSRA Award and as a co-author for several award papers. He was elected as the IEEE CAS Distinguished Lecturer in 2005. He was a Vice President in the Signal Processing Society and IEEE Signal Processing Society Distinguished Lecturer. He is now a Fellow of the Academy of Engineering, Singapore, a Life Fellow of IEEE and a Fellow of IES.